Characterisation of the ionic products arising from electron photodetachment of simple dicarboxylate dianions

Abstract
Much of what we currently understand about the structure and energetics of multiply charged anions in the gas phase is derived from the measurement of photoelectron spectra of simple dicarboxylate dianions. Here we have employed a modified linear ion-trap mass spectrometer to undertake complementary investigations of the ionic products resulting from laser-initiated electron photodetachment of two model dianions. Electron photodetachment (ePD) of the [M-2H]2- dianions formed from glutaric and adipic acid were found to result in a significant loss of ion signal overall, which is consistent with photoelectron studies that report the emission of slow secondary electrons (Xing et al., 2010 [20]). The ePD mass spectra reveal no signals corresponding to the intact [M-2H]•- radical anions, but rather[M-2H-CO2]'- ions are identified as the only abundant ionic products indicating that spontaneous decarboxylation follows ejection of the first electron. Interestingly however, investigations of the structure and energetics of the [M-2H-CO2]•- photoproducts by ion-molecule reaction and electronic structure calculation indicate that (i) these ions are stable with respect to secondary electron detachment and (ii) most of the ion population retains a distonic radical anion structure where the radical remains localised at the position of the departed carboxylate moiety. These observations lead to the conclusion that the mechanism for loss of ion signal involves unimolecular rearrangement reactions of the nascent [M-2H]•- carbonyloxyl radical anions that compete favourably with direct decarboxylation. Several possible rearrangement pathways that facilitate electron detachment from the radical anion are identified and are computed to be energetically accessible. Such pathways provide an explanation for prior observations of slow secondary electron features in the photoelectron spectra of the same dicaboxylate dianions.

Keywords
dicarboxylate, simple, photodetachment, dianions, electron, ionic, arising, products, characterisation

Disciplines
Medicine and Health Sciences | Social and Behavioral Sciences

Publication Details
Kirk, B. B., Trevitt, A. J., Poad, B. L. and Blanksby, S. J. (2013). Characterisation of the ionic products arising from electron photodetachment of simple dicarboxylate dianions. International Journal of Mass Spectrometry, 351, 81-94.

Characterisation of the ionic products arising from electron photodetachment of simple dicarboxylate dianions.

Benjamin B. Kirk[a,b], Adam J. Trevitt[a,b], Berwyck L. J. Poad[a], Stephen J. Blanksby[a,b,*]

[a]*School of Chemistry, University of Wollongong, NSW 2522, Australia*
[b]*ARC Centre of Excellence for Free Radical Chemistry and Biotechnology, University of Wollongong, NSW 2522, Australia*

Abstract

Much of what we currently understand about the structure and energetics of multiply-charged anions in the gas phase is derived from the measurement of photoelectron spectra of simple dicarboxylate dianions. Here we have employed a modified linear ion-trap mass spectrometer to undertake complementary investigations of the ionic products resulting from laser-initiated electron photodetachment of two model dianions. Electron photodetachment (ePD) of the $[M - 2H]^{2-}$ dianions formed from glutaric and adipic acid were found to result in a significant loss of ion signal overall which is consistent with photoelectron studies that report the emission of slow secondary electrons [Xing *et al. J. Phys. Chem. A* **2010**, *114*, 4524]. The ePD mass spectra reveal no signals corresponding to the intact $[M - 2H]^{\bullet-}$ radical anions but rather $[M - 2H - CO_2]^{\bullet-}$ ions are identified as the only abundant ionic products indicating that spontaneous decarboxylation follows ejection of the first electron. Interestingly however, investigations of the structure and energetics of the $[M - 2H - CO_2]^{\bullet-}$ photoproducts by ion-molecule reaction and electronic structure calculation indicate that (i) these ions are stable with respect to secondary electron detachment and (ii) most of the ion population retains a distonic radical anion structure where the radical remains localised at the position of the departed carboxylate moiety. These observations lead to the conclusion that the mechanism for loss of ion signal involves unimolecular rearrangement reactions of the nascent $[M - 2H]^{\bullet-}$ carbonyloxyl radical anion that compete favourably with direct decarboxylation. Several possible rearrangement pathways that facilitate electron detachment from the radical anion are identified and are computed to be energetically accessible. Such

pathways provide an explanation for prior observations of slow secondary electron features in the photoelectron spectra of the same dicaboxylate dianions.
Keywords: Multiply charged anions, electron photodetachment, electrospray ionisation, ion-trap mass spectrometry

1. Introduction

Multiply-charged anions (MCA) are ubiquitous in the condensed phase where solvent and counter-ions serve to stabilise individual charges and minimise repulsive interactions. In the gas phase however, shielding of the repulsive interactions between like-charges is minimised and MCAs are destabilised towards electron detachment or dissociation [1, 2]. As such, many chemists were initially sceptical that gas-phase MCAs could be generated at all and the first reports of the detection of atomic oxygen and halogen dianions by Stuckey and Kiser [3] was warily questioned [4]. While subsequent investigations appeared to confirm this result [5, 6], later studies were unable to find evidence for atomic dianions [7–9]. Experiments soon demonstrated however, that molecular dianions could be generated in the gas phase, paving the way for a series of pioneering studies of this phenomenon. Bowie and Stapleton were the first to generate molecular dianions by secondary electron capture under chemical ionization conditions in a sector mass spectrometer [10]; while Compton and co-workers employed ion-sputtering and anion electron capture to produce fullerene and other carbon-cluster dianions [11–13]. With the advent of electrospray ionisation (ESI) [14] however, the preparation of gas-phase MCAs became almost immediately routine. The contemporary mass spectrometrist will now commonly observe dianions (and even much higher charge states) upon negative ion ESI analysis of biomolecules such as proteins, peptides, oligonucleotides and even some lipids [15–17]; although little thought is usually given to the structure and energetics that underpin the stability of these remarkable ions in the gas phase.

*Corresponding author
Email address: blanksby@uow.edu.au (Stephen J. Blanksby)

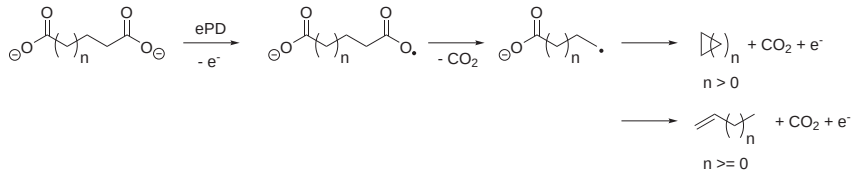

Scheme 1: Putative fragmentation pathways proposed by Xing *et al.* to account for both high and near-zero kinetic energy electrons observed during photoelectron spectroscopy experiments of aliphatic dicarboxylate dianions [20].

Much of what we now understand about the structure and stability of gas-phase MCAs has arisen from experiments undertaken by Wang and co-workers who successfully coupled ESI with photoelectron spectroscopy (PES). In a series of elegant studies, a collection of simple dicarboxylate dianions of the form $[O_2C{-}(CH_2)_n{-}CO_2]^{2-}$ (where n = 2 - 8) were formed by ESI of aliphatic diacids and subjected to laser photodetachment [18, 19]. The detection of energetic photoelectrons in these experiments was consistent with the formation of $[O_2C{-}(CH_2)_n{-}CO_2]^{\bullet-}$ radical anions - that incorporate a reactive carbonyloxyl radical motif - but the ionic products arising from the irradiation event could not be directly detected or mass-analysed on this apparatus. In their recent photoelectron imaging study of the same suite of dianions, Wang and co-workers also investigated a second population of electrons appearing at near-zero kinetic energy [1, 20, 21]. This spectral signature was assigned to electron autodetachment subsequent to decarboxylation of the nascent carbonyloxyl radical as illustrated in Scheme 1. In essence, two photoelectrons are generated from one photoexcited dianion, the first with 1 - 3 eV kinetic energy (depending on the length of the chain) and the second electron with near-zero kinetic energy.

The first step in the process, described in Scheme 1, is facile decarboxylation of the carbonyloxyl radical intermediate and is consistent with the behaviour of simple neutral carbonyloxyl radicals that are known to undergo spontaneous decarboxylation [22–25]. Although there is general agreement that carbonyloxyl radicals decompose *via* loss of carbon dioxide, estimates of their lifetimes of these intermediates vary. Results from neutralisation-reionisation mass spectrometry studies carried out by Schröder *et al.* suggested that the lifetime of the acetyloxyl radical ($CH_3CO_2^{\bullet}$) in the gas phase could be as little as 100 ps,

while a photoelectron photofragment coincidence investigation by Lu and Continetti indicated this species could be stable for microseconds [22]. In solution too, estimates for the lifetimes of $RCO_2^{\bullet}$ radicals range from 10^{-6} - 10^{-12} seconds depending on the measurement techniques and the structure of the R-group [23–25]. Given the potentially wide window of lifetimes for the carbonyloxyl radical anions $[O_2C{-}(CH_2)_n{-}CO_2]^{\bullet-}$ formed in the PES experiments described above, it is interesting to consider whether unimolecular rearrangement may compete with the prompt decarboxylation indicated in Scheme 1. Indeed, competition between rearrangement and decarboxylation channels for carbonyloxyl radicals was suggested by Schröder following his neutralisation studies of alkyl carboxylate anions [26]. In the context of photodetached dicarboxylate dianions, rearrangement of the nascent carbonyloxyl radical anions could lead to a stable (and thus persistent) isomeric form or alternatively present a pathway for direct detachment of the secondary electron. The latter would represent an alternative pathway to that outlined as the second step in Scheme 1, which points to unimolecular rearrangement of the carboxylate alkyl radical being the driver of electron detachment. To the authors' knowledge however, the structure and stability of such carboxylatoalkyl radical anions has not been investigated and thus the likelihood of such electron detachment reactions is unknown.

While PES has provided critical insights into the electronic structure of MCAs, determing the ionic products from photodetachment of simple dianions has received less attention. Ion-trap mass spectrometry coupled with laser photolysis has previously been employed to generate and interrogate the ionic products arising from the photo-excitation of ions [27–31]. In the present study, we have selected two dicarboxylate dianions from the homologues series previously studied by PES [1, 20, 21]. These two dianions, of the form $[O_2C{-}(CH_2)_n{-}CO_2]^{2-}$ where n = 3 and 4, have been generated by ESI of precursor diacids and then isolated in a specially modified linear ion-trap mass spectrometer, where they have been subjected to 266 nm laser irradiation. The results presented herein demonstrate that neither $[O_2C{-}(CH_2)_n{-}CO_2]^{\bullet-}$, nor rearranged isomers, are detected following photodetachment but rather the major photoproduct pathway results in a loss of ion signal. Product ions arising from spontaneous decarboxylation are detected, but both experiment

and electronic structure calculations suggest that they do not undergo electron detachment processes. Electronic structure calculations further elucidate accessible electron detachment pathways directly from the initially formed $[O_2C{-}(CH_2)_n{-}CO_2]^{\bullet-}$ radical anion intermediates. These processes can account for the loss of ion signal observed in these experiments as well as provide an explanation for the near-zero kinetic energy electrons previously detected by PES.

2. Experimental

2.1. Materials

2-Bromovaleric acid, sodium iodide, glutaric and adipic acid were purchased from Sigma-Aldrich (St. Louis, MO). Ajax branded HPLC-grade methanol, acetone and ammonia solution (28%) were purchased from Thermo Fisher Scientific (Scoresby, VIC, Australia). 2-Iodovaleric acid was generated from 2-bromovaleric acid by Finkelstein reaction with sodium iodide in acetone [32] and used without further purification.

2.2. Mass Spectrometry

Experiments were performed on a modified Thermo Fisher Scientific LTQ (San Jose, CA) linear quadrupole ion-trap mass spectrometer [33] fitted with a conventional IonMax electrospray ionisation source and operating Xcalibur 2.0 SUR1 software. Typical instrumental settings in negative ion mode were: spray voltage: -3.5 kV; capillary temperature: 200 - 250 ℃); sheath gas flow: 10 - 30 (arbitrary units); sweep and auxillary gas flow: 0 - 10 (arbitrary units). A methanolic solution of the precursor was basified with aqueous ammonia and was infused at 3-5 µL min^{-1} *via* electrospray ionisation to yield $[M - H]^-$ and $[M - 2H]^{2-}$ ions in the case of diacids. In photodetachment experiments, the $[M - 2H]^{2-}$ dianion generated from the diacids was isolated and subjected to a single 266 nm laser pulse timed to coincide with the activation step of the MS cycle. For collision-induced dissociation experiments, ions were mass-selected with a window of 2 - 5 Th, using a q-parameter of 0.250, and the fragmentation energy applied was typically 10 - 45 (arbitrary units) with an excitation time of 30 ms (unless otherwise noted).

2.3. Ion-molecule reactions

The process of measuring ion-molecule reactions in this mass spectrometer has been described in detail previously [34]. Briefly, the atmospheric pressure ionisation source allows adventitous oxygen to diffuse into the ion trap region of the mass spectrometer. Previous studies of the 3-carboxylatoadamantyl + O_2 reaction have established a second-order rate constant for this reaction, which is now used as a calibrant reaction to determine the O_2 concentration [34]. The temperature of the vacuum manifold has previously been measured at 307 ± 1 K [34], which is taken as the effective temperature for the ion-molecule reactions measured herein. Reaction times of 0.03 - 10 000 ms are set using the excitation time parameter with the collision energy set at 0 (arbitrary units) within the mass spectrometer control software. Each time point on the kinetic measurement is the average of at least 30 scans. Plotting the natural logarithm of the parent ion abundance at each time-point (R_t) relative to its initial concentration (R_0) results in a straight line with slope $-k_1$ (Equation 1). The second-order rate constant is calculated from the pseudo-first order rate constant and the measured concentration of O_2 according to Equation 2. Finally, the reaction efficiency is calculated as described in Equation 3, where k_2 is the second-order rate constant and k_{col} is calculated using Trajectory collision rate theory (this value is the same as both the Langevin and Average Dipole Orientation (ADO) collision rates when the neutral has no dipole moment, such as O_2).

$$\ln \frac{[R]_t}{[R]_0} = -k_1 + c \tag{1}$$

$$k_2 = \frac{k_1}{[O_2]} \tag{2}$$

$$\phi = \frac{k_2}{k_{col}} \tag{3}$$

Due to charge-loss channels observed during these experiments, R_0 is taken as the total ion count measured at 30 ms, therefore, the rate constant calculated is not normalised at each

time-point and large fluctuations in the parent ion signal may increase the random error. Random errors in these measurments were typically $2\sigma < 10\%$ where σ is the standard deviation obtained from the least-squares fit to the psuedo-first order decay. Systematic errors arise due to ions that form with a m/z less than the low-mass cuttoff (15 - 25 Th during isolation of dianions presented herein in low-mass mode and 50 Th in normal-mass range mode). Overall, an upper limit for the absolute uncertainties of 50% has been estimated for the measured rate constants, while random uncertainties in the measurements are typically less than 10%.

2.3.1. Electron Photodetachment

The modification of the linear ion-trap to accommodate introduction of a laser pulse into the ion-trapping region is similar to previous implementations [35, 36], and our specific instrumentation has been described in detail elsewhere [37]. Briefly, a 2.75 in. quartz viewport is attached to the backplate of the spectrometer vacuum housing with a CF flange to allow transmission of 266 nm (fluence = 34 mJ cm^{-2}) laser pulses generated by a flashlamp-pumped Nd:YAG laser (Minilite II, Continuum, Santa Clara, CA). The laser pulse is directed through an aperture in the back lens of the ion-trap assembly and adjusted to optimise the overlap with the ion cloud. The laser flashlamp is triggered by a TTL pulse generated by the mass spectrometer at the beginning of a typical MS^n ion activation step. In these ePD experiments, the activation energy is set to 0 and thus all product ions arise due to excitation by the single laser pulse. Additionally, ePD was confirmed to proceed by a single photon excitation by plotting photoproduct abundance against laser power to yield a straight line (see Supporting Information, Figures S1 and S2). Photodetachment yield was determined by measuring interleaved laser on/off spectra over 500 scans to minimise the effect of ion signal and laser power fluctuations [38]. It should be noted that a marked difference in detection efficiency has been observed between monoanions and dianions, with a significant bias towards the latter, during reaction of dianions with methyl iodide; therefore, comparisons between dianion and monoanion abundances should be made with caution.

2.4. Computational Chemistry

All calculations were undertaken using the hybrid density functional theory M06-2X method and the 6-311++G(d,p) basis set within the GAUSSIAN09 suite of programs [39]. All stationary points on the potential energy surface were characterised as either minima (no imaginary frequencies) or transition states (one imaginary frequency) by calculation of the frequencies using analytical gradient procedures. All reported energies include unscaled zero-point energy corrections. Transition states between minima were confirmed by calculation of the intrinsic reaction coordinate (IRC).

Vibrational partition functions (Q_{vib}) were calculated using a simple harmonic approximation employing Equations 4 and 5, where q^{ν} is the vibration partition function for each normal mode, $\tilde{\nu}$ is the calculated vibrational frequency of the normal mode, h is the Planck constant, k_B is the Boltzmann constant and T is temperature (298.15 K) [40–43].

$$Q_{vib} = q^{\nu}(0)q^{\nu}(1)...q^{\nu}(n) \quad (4)$$

$$q^{\nu} = \frac{1}{1 - e^{\frac{-hc\tilde{\nu}}{k_B T}}} \quad (5)$$

3. Results

3.1. Photodetachment of the [M-2H]$^{2-}$ dianion of glutaric acid ($\boldsymbol{G}^{2-}$)

The [M - 2H]$^{2-}$ dianion ($\mathbf{G}^{2-}$) at *m/z* 65 formed by ESI of a methanolic solution of glutaric acid was mass-selected in the ion trap. The mass spectrum measured after isolation of this ion for 30 ms is presented in Figure 1(a). Product ions arise at *m/z* 74, 86 and 131 that are assigned as [**G** + H_2O]$^{2-}$, [**G** - CO_2]$^{\bullet-}$ and [**G** + H]$^{-}$, respectively. The presence of an ion-water cluster at *m/z* 74 suggests that the [**G** + H]$^{-}$ at *m/z* 131 arises due to proton transfer from background water, methanol or other proton donors present within the ion-trapping region of the mass spectrometer. Indeed, increasing the isolation time to 5000 ms results in a significant increase in the abundance of these ions providing strong evidence that both result from ion-molecule reactions with background neutrals present in the trap (see Supporting Information, Figure S3). The relative abundance of the [**G** - CO_2]$^{\bullet-}$ ion at

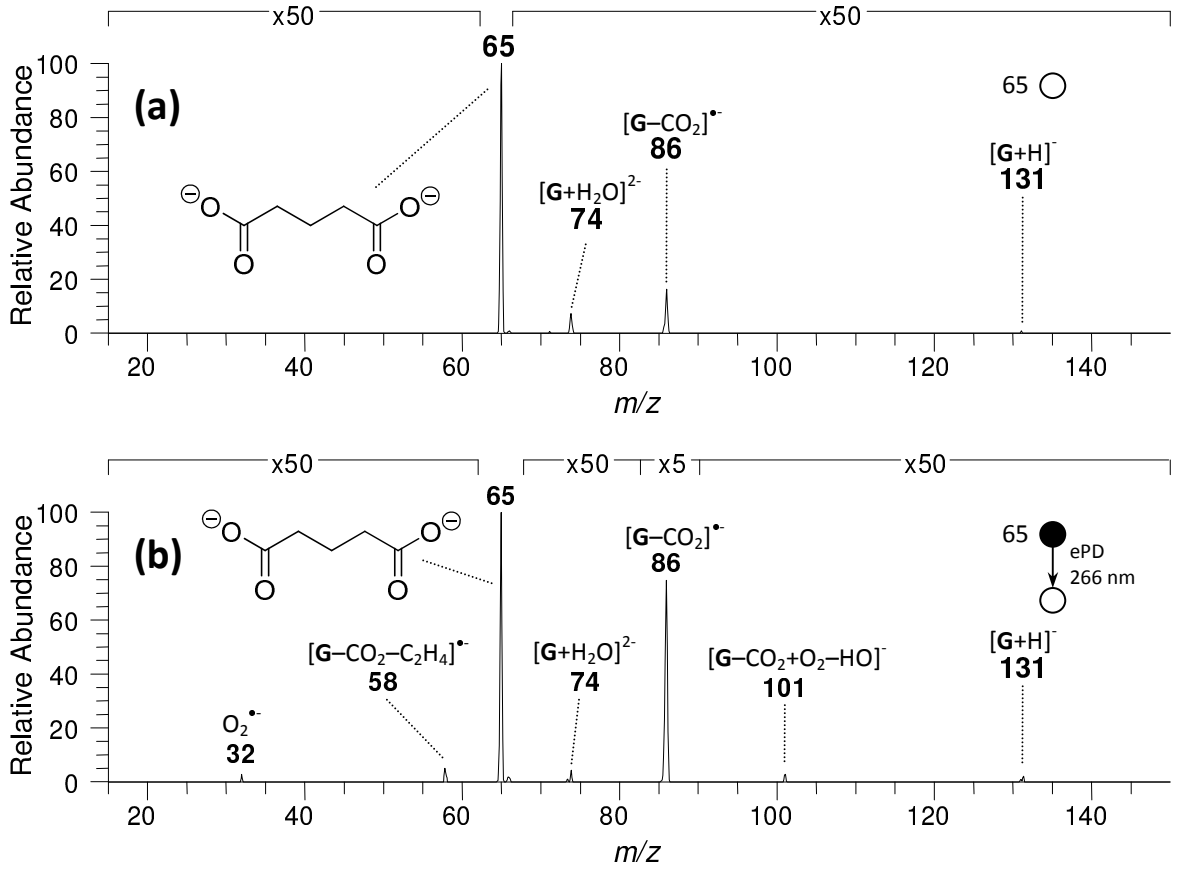

Figure 1: Mass spectrum measured after (a) isolation of the [M - 2H]$^{2-}$ dianion ($\mathbf{G}^{2-}$) at m/z 65 formed by ESI of a methanolic solution of glutaric acid, and (b) 266 nm electron photodetachment (ePD) of the isolated m/z 65 dianion.

173 *m/z* 86 may be decreased by increasing the isolation width suggesting this ion arises due
174 to excitation of the precursor ion during the isolation process, resulting in decarboxylation
175 with concomitant electron detachment; a process well-known following CID of dicarboxylate
176 dianions [44, 45].

177 When $\mathbf{G}^{2-}$ is subjected to a single 266 nm laser pulse the total ion count decreases by
178 *ca.* 50%, indicating either a large quantity of photoproducts reside below 15 Th (*i.e.* the
179 low-mass limit of the instrument while isolating *m/z* 65), or alternatively, detachment of a
180 second electron yields neutral products that cannot be detected by mass spectrometry. The
181 former is unlikely, while the latter is consistent with observation of near-zero kinetic electrons
182 in the PES experiments of Xing *et al.* [20]. We point out here, that the magnitude of the
183 electron loss pathway(s) cannot be quantified due to a significant detection bias towards
184 dianions over monoanions. Despite this limitation, the low recovery of ionic photoproducts
185 overall suggests that secondary electron emission is a major product channel, arising from
186 the inital ePD.

187 The glutarate radical anion ($\mathbf{G}^{\bullet-}$) is not detected at *m/z* 130 following ePD, consistent
188 with the expected short lifetime of carbonyloxyl radicals (*i.e.* 10^{-6} - 10^{-12} s) [22–24, 26] rel-
189 ative to the timescale for ion detection in our experiments (*ca.* 100 ms). Furthermore, it ex-
190 cludes rearrangement of the carbonyloxyl radical to a stable isomer. This leaves two possible
191 fates for the nascent radical anion: (a) prompt decarboxylation with subsequent secondary
192 electron detachment from an intermediate $[\mathbf{G} - CO_2]^{\bullet-}$ radical anion, or (b) rearrangement
193 of $\mathbf{G}^{\bullet-}$ itself, resulting in direct electron detachment, perhaps coupled with concerted de-
194 carboxylation. The former rationale can be explored by further examination of Figure 1(b)
195 which reveals a major $[\mathbf{G} - CO_2]^{\bullet-}$ ion at *m/z* 86, assigned as 3-carboxylatopropyl radical
196 anion (**3-CP**). While *m/z* 86 was identified during isolation of the precursor dianion (Figure
197 1a), subjecting $\mathbf{G}^{2-}$ to ePD results in an marked enhancement in the abundance of this ion
198 (Figure 1b). As depicted in Scheme 1, Xing *et al.* previously postulated that near-zero
199 kinetic energy electrons arise after decarboxylation of the nascent carbonyloxyl radical *via*
200 β-scission, hydrogen atom transfer, or cyclisation, all resulting in ejection of $CO_2 + e^-$ [20].
201 Our ability to isolate this ion population over long timescales (> 1000 ms) suggests the

$[\mathbf{G}$ - $CO_2]^{\bullet-}$ ion is stable with respect to electron detachment and thus, these pathways may not be significantly contributing to ion loss (or secondary electron emission). Nevertheless, electronic structure calculations at the M06-2X/6-311++G(d,p) level of theory for the possible rearrangement and decomposition pathways of **3-CP** were undetaken and the results are depicted in Scheme 2. While hydrogen atom transfer channels (iii) and (iv) to form the isomeric radicals **1-CP** and **2-CP**, respectively, are exothermic overall, they have significant barriers that reside at 32.9 and 34.8 kcal mol^{-1} above $\mathbf{G}^{\bullet-}$. 1,3-Cyclisation of **3-CP** to give cyclopropane (v) requires surmounting a higher barrier of 35.1 kcal mol^{-1}. The lowest barriers to rearrangement from **3-CP** are β-scission (vi) at 26.7 kcal mol^{-1} and γ-lactonisation (vii), with a barrier at 29.2 kcal mol^{-1} above $\mathbf{G}^{\bullet-}$. As postulated, these computational and experimental observations confirm that secondary electron detachment from **3-CP** is unlikely to significantly contribute to the observed loss of ion signal following ePD.

These results suggest secondary electron emission may instead be arising directly from the nascent $\mathbf{G}^{\bullet-}$ radical anion. Two low-energy reaction channels were identified: 1,5-hydrogen atom transfer and γ-lactonisation. The barrier for 1,5-hydrogen atom transfer (viii) resides at only 5.1 kcal mol^{-1} above $\mathbf{G}^{\bullet-}$ to form the 1-carboxy-3-carboxylato-2-propyl radical anion with a reaction exothermicity of -8.9 kcal mol^{-1}. Significantly, the barrier for direct γ-lactonisation of $\mathbf{G}^{\bullet-}$ (ix) is competitive with hydrogen atom transfer, residing at only 5.4 kcal mol^{-1}, to form γ-butyrolactone + CO_2 + e^- with an overall reaction exothermicity of -4.7 kcal mol^{-1}. In both cases, rotation of the carboxylate group must occur prior to reaction; however, this rotation is directly coupled with decarboxylation. The intrinsic reaction coordinate calculated for the transition state of 1,5-hydrogen atom transfer (presented in Supporting Information, Figure S7), for example, contains an inflection point where this rotation joins the reaction path. The reactant optimisation minimises to the **3-CP** + CO_2 ion-dipole complex at -7.2 kcal mol^{-1} below $\mathbf{G}^{\bullet-}$. These calculations therefore suggest that decarboxylation will directly compete with hydrogen atom transfer. Taken together, experimental and theoretical evidence suggests the observed ion signal loss arises due to direct rearrangement of the nascent $\mathbf{G}^{\bullet-}$ and further, accounts for the near-zero kinetic energy

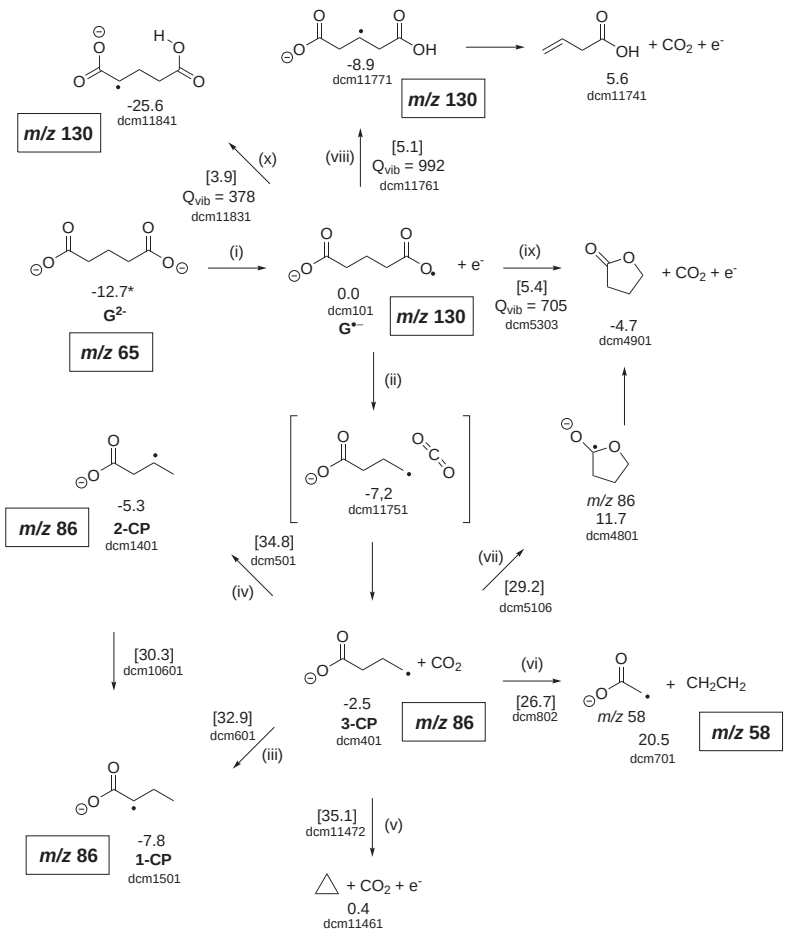

Scheme 2: Putative fragmentation pathways of the glutarate dianion following electron photodetachment (ePD). Calculated at the M06-2X/6-311++G(d,p) level of theory with unscaled zero-point energy correction. All energies are given in kcal mol^{-1} and are reported relative to $\mathbf{G}^{\bullet-}$. Energies include all neutral fragments along the reaction channel (*i.e.*, the energy of the initial carbon dioxide is included). The codes provided beneath each structure are references to the raw geometry and energy data reported in Supporting Information. *Energy was calculated from the electron binding energy measured by Wang *et al.* [46]

electrons reported by Xing *et al.* [20].

*3.2. Identification of the [**G** - CO_2]$^-$ ion formed after ePD of glutarate dianion (**G**$^{2-}$).*

The [**G** - CO_2]$^{\bullet-}$ ion that arises at *m/z* 86 ion is most certainly a carboxylatopropyl radical anion; however, the location of the unpaired electron may vary depending on whether the **3-CP** initially generated isomerises to either the 1-carboxylatoprop-2-yl (**2-CP**) or 1-carboxylatoprop-1-yl (**1-CP**) radical anion *via* hydrogen atom transfer. As shown in Scheme 2, the barrier to hydrogen atom transfer from **3-CP** to the lowest energy **1-CP** isomer (iii) was calculated at 35.4 kcal mol^{-1} above **3-CP**. The barrier to β-scission (vi) is lower by 6.2 kcal mol^{-1} at 29.2 kcal mol^{-1} and there is evidence of a small contribution from this channel at *m/z* 58 in the mass spectrum presented in Figure 1(b). It was therefore prudent to test for isomerisation of the nascent alkyl carboxylate radical anion.

Reactions of alkyl radicals with molecular oxygen (O_2) have previously been used as a diagnostic for distonic radical ions [47, 48]. In earlier studies, we have shown that molecular oxygen adds to distonic radical anions to generate an [M + 32]$^-$ ion, assigned as an alkylperoxyl radical, which may degrade to form either an [M + 15]$^-$ ion assigned as hydroxyl radical loss to form a ketone or epoxide, or an [M - 1]$^-$ ion arising due to loss of hydroperoxyl radical from the nascent alkylperoxyl radical [37, 49, 50]. In contrast, for a cross-conjugated α-carboxylate radical anion, reaction with O_2 leads primarily to formation of carbonate radical anion ($CO_3^{\bullet-}$) with *m/z* 60 [37, 49]. In the present experiments, should **3-CP** be formed after decarboxylation of **G**$^{\bullet-}$ and rearrange to the lower energy **1-CP** isomer, we would expect its reaction in the presence of O_2 to result in formation of $CO_3^{\bullet-}$. Conversely, should **3-CP** thermalise without isomerisation, reaction in the presence of O_2 should lead to formation of a mixture of ions that may include [M + 32], [M + 15] and [M - 1] at *m/z* 118, 101 and 85, respectively.

We have therefore investigated the reaction of the nascent carboxylatopropyl radical anion with O_2. Allowing the [**G** - CO_2]$^{\bullet-}$ ion at *m/z* 86 to react with O_2 (present in background concentrations) for 4000 ms resulted in the mass spectrum shown in Figure 2. Plotting the natural logarithm of the *m/z* 86 ion decay against time demonstrated that this

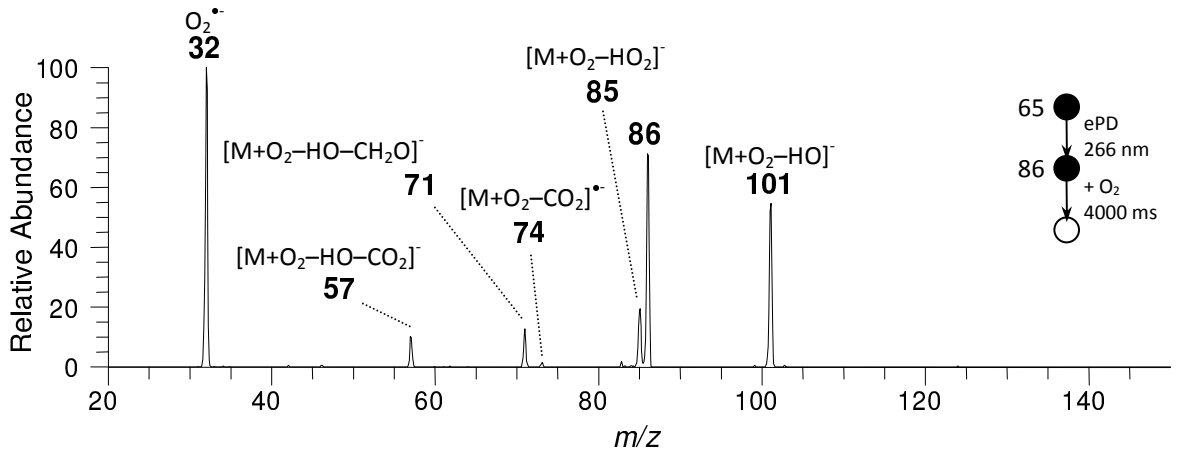

Figure 2: Mass spectrum measured after reaction of the $[\mathbf{G}$ - $CO_2]^{\bullet-}$ ion at *m/z* 86 generated by electron photodetachment (ePD) of the glutarate dianion ($\mathbf{G}^{2-}$, *m/z* 65) in the presence of O_2 for 4000 ms.

reaction follows pseudo-first order kinetics and suggests there is a single isomer present in this ion population. Using a calibration reaction to detemine the concentration of O_2 (*vide supra*), a second-order rate constant was measured for this reaction at $k_2(R + O_2)$ = 7.1 ± 0.3 x 10^{-11} molecules^{-1} cm^3 s^{-1}, which represents a reaction efficiency of 12% (k_{coll} = 6.1 x 10^{-10} molecules^{-1} cm^3 s^{-1}). Interestingly, the total ion count decreases significantly after reaction of the *m/z* 86 ion with O_2. Calculation of the product branching ratios indicate low-mass ions or product channels that result in electron detachment account for 39% of reaction products. Note that measurement of the ion count is now quantitative as we are comparing ion abundances of monoanions only. Importantly, an ion of *m/z* 60, a key indicator for the presence of the α-carboxylate isomer **1-CP**, is entirely absent suggesting that this isomerisation has not occurred [37, 49]. Instead the mass spectrum reveals a dominant ion at *m/z* 32, assigned as superoxide ($O_2^{\bullet-}$). In addition, a range of ions including $[M + 15]^-$, $[M - 1]^-$, $[M-12]^-$, $[M - 15]^-$ and $[M - 29]^-$ ions arise at *m/z* 101, 85, 74, 71 and 57, assigned as addition of O_2 to form the nascent peroxyl radical with subsequent loss of HO, HO_2, CO_2, HO + CH_2O and HO + CO_2, respectively. The presence of these ions is consistent with the ions at *m/z* 86 being a distonic carboxylatopropyl radical anion. The absence of **1-CP** suggests that **2-CP** is similarly not formed, as the barrier for this 1,3-hydrogen atom transfer is higher still than the 1,4-hydrogen atom transfer to form **1-CB**

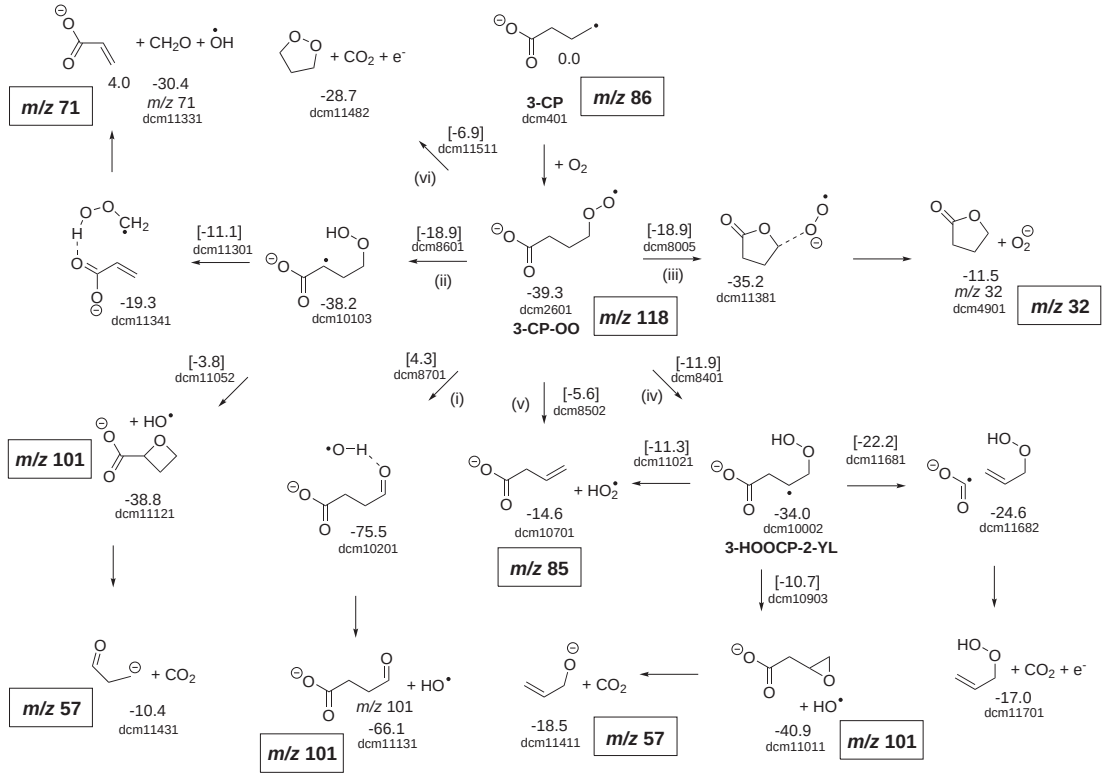

Scheme 3: Potential reaction pathways of the 3-carboxylpropyl radical anion + O_2 reaction. Calculated at the M06-2X/6-311++G(d,p) level. Energies are reported in kcal mol^{-1} and include unscaled zero-point energy corrections. The codes provided beneath each structure are references to the raw geometry and energy data reported in Supporting Information.

(Scheme 2). Taken together, these data suggest the only isomer present in the *m/z* 86 [**G** - CO_2]$^{\bullet-}$ ion population is **3-CP**.

Electronic structure calculations of putative reaction channels at the M06-2X/6-311++G(d,p) level of theory reveal all reaction products arising from the **3-CP** + O_2 reaction are energetically accessible (Scheme 3). Addition of O_2 results in the 3-carboxylatopropylperoxyl radical anion (**3-CP-OO**) with a reaction exothermicity of -39.3 kcal mol^{-1}. The abundance of potential reaction channels accessible to the nascent peroxyl radical provides a clear explanation for the absence of an [M + O_2]$^{\bullet-}$ ion at *m/z* 118 in Figure 2. 1,4-Hydrogen atom transfer to generate 3-carboxypropanone + HO (i) is unlikely to occur due to a barrier that resides 4 kcal mol^{-1} above the energy of the reactants. The lowest energy pathways are 1,6-hydrogen atom transfer (ii) and γ-lactonisation (iii) with isoenergetic transition states -18.9

kcal mol^{-1} below the entrance channel. 1,6-hydrogen atom transfer (ii) results in formation of the 1-carboxylato-1-hydroperoxyl-3-propyl radical anion, exothermic overall by 38.2 kcal mol^{-1}. This intermediate may either eject HO through a barrier of 34.4 kcal mol^{-1} to form 1-carboxylato-1,3-epoxypropane residing -38.8 kcal mol^{-1} below the entrance channel, or proceed *via* β-scission with a barrier of 27.1 kcal mol^{-1} to form an ion-dipole complex between propenoate anion and the hydroperoxylmethyl radical 19.3 kcal mol^{-1} below the reactants. While no transition state was calculated, it is assumed this ion-dipole complex may eject CH_2O, then HO to generate propenoate anion with an overall reaction exothermicity of -30.4 kcal mol^{-1}, accounting for the ion that arises at *m/z* 71 in Figure 2. The loose barrier to β-scission is both lower in energy and entropically favoured with respect to the tight barrier to epoxidation, therefore, one would not expect the epoxidation channel to contribute significantly to the population of *m/z* 101 ions, or after decarboxylation, the ions of *m/z* 57. In comparison, γ-lactonisation (iii) results in formation of an ion-dipole complex 35.2 kcal mol^{-1} below the entrance channel; γ-butyrolactone and $O_2^{\bullet-}$ are held together by 23.7 kcal mol^{-1} and when separated form the individual products with an overall reaction exothermicity of -11.5 kcal mol^{-1}, accounting for facile formation of $O_2^{\bullet-}$ at *m/z* 32.

Two pathways may proceed *via* 1,5-hydrogen atom transfer; concerted 1,5-hydrogen atom transfer and HO_2 ejection requires 33.7 kcal mol^{-1} to form propenoate anion + HO_2 at -14.6 kcal mol^{-1} below the energy of the reactants, while 1,5-hydrogen atom transfer to form the 1-carboxylato-3-hydroperoxyl-2-propyl radical anion (**3-HOOCP-2-YL**) has a barrier of 27.4 kcal mol^{-1} and overall reaction exothermicity of -28.6 kcal mol^{-1}. The latter may either eject HO_2 through a barrier of 17.3 kcal mol^{-1}, or release HO, which requires 17.9 kcal mol^{-1} to form 1-carboxylato-2-epoxypropane + HO with a reaction exothermicity of -40.9 kcal mol^{-1}. The former accounts for the ion signal at *m/z* 85, while the latter the ions at *m/z* 101. Decarboxylation of the 1,2-epoxide results in formation of prop-2-en-1-olate anion residing -18.5 kcal mol^{-1} below the entrance channel to account for the ion of *m/z* 57. Alternatively, the intermediate may undergo β-scission with a barrier residing at -22 kcal mol^{-1} to form an ion-dipole complex at -24.8 kcal mol^{-1} that may release 3-hydroperoxylpropene + $CO_2 + e^-$ with a reaction exothermicity of -17.0 kcal mol^{-1}. Significantly, this reaction channel results

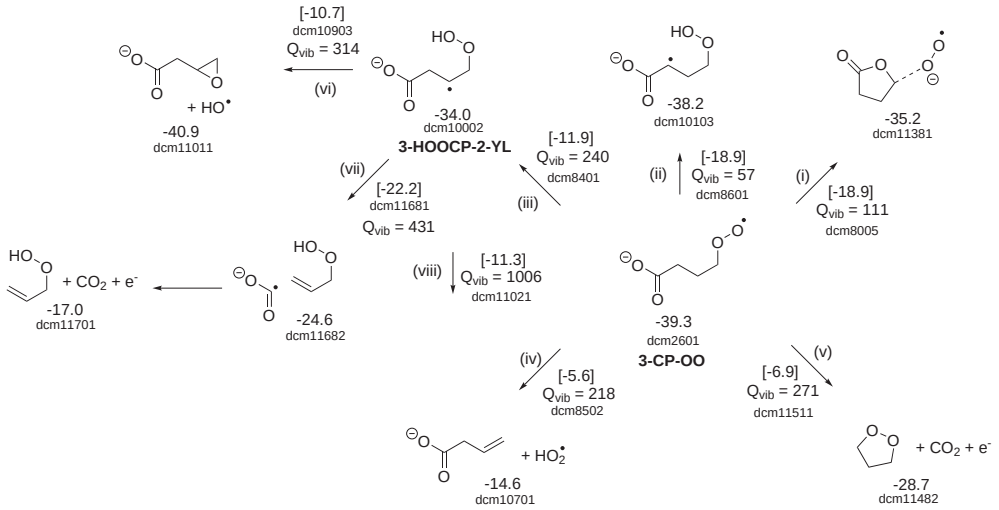

Scheme 4: Potential reaction pathways of the 3-carboxylatopropylperoxyl radical anion with estimated vibrational partition functions (Q_{vib}). Calculated at the M06-2X/6-311++G(d,p) level. Energies include unscaled zero-point energy corrections. The codes provided beneath each structure are references to the raw geometry and energy data reported in Supporting Information.

in neutral products not detected by mass spectrometry. Similarly, the nascent **3-CP-OO** radical anion may cyclise to form a cyclic peroxide (v). The barrier to 1,5-cyclisation of **3-CP-OO** (v) was calculated to reside at -6.9 kcal mol^{-1} with respect to the reactants to form 1,2-dioxolane + CO_2 + e^- with an overall exothermicity of -28.7 kcal mol^{-1} below the reactants again leading to neutral products that could not be detected.

When multiple reaction channels are accessible during radical reactions, estimating the vibrational partition functions (Q_{vib}) of key transition states can be informative, where a larger value indicates a greater density of states with which to accomodate transmission through the barrier [40–42]. While the barriers to γ-lactonisation (i) and 1,6-hydrogen atom transfer (ii) are isoenergetic, the 5-membered ring transition state for γ-lactonisation is the entropically favoured pathway, as indicated by the larger Q_{vib} for this transition state (depicted in Scheme 4) and demonstrated by the dominant $O_2^{\bullet-}$ ion at m/z 32 in Figure 2. Both 1,5-hydrogen atom transfer (iii) and concerted 1,5-hydrogen atom transfer and HO_2 ejection (iv) have even higher Q_{vib} values. As these transition states are also energetically accessible, they compete with (i) and (ii); 1,5-hydrogen atom transfer reaction pathways

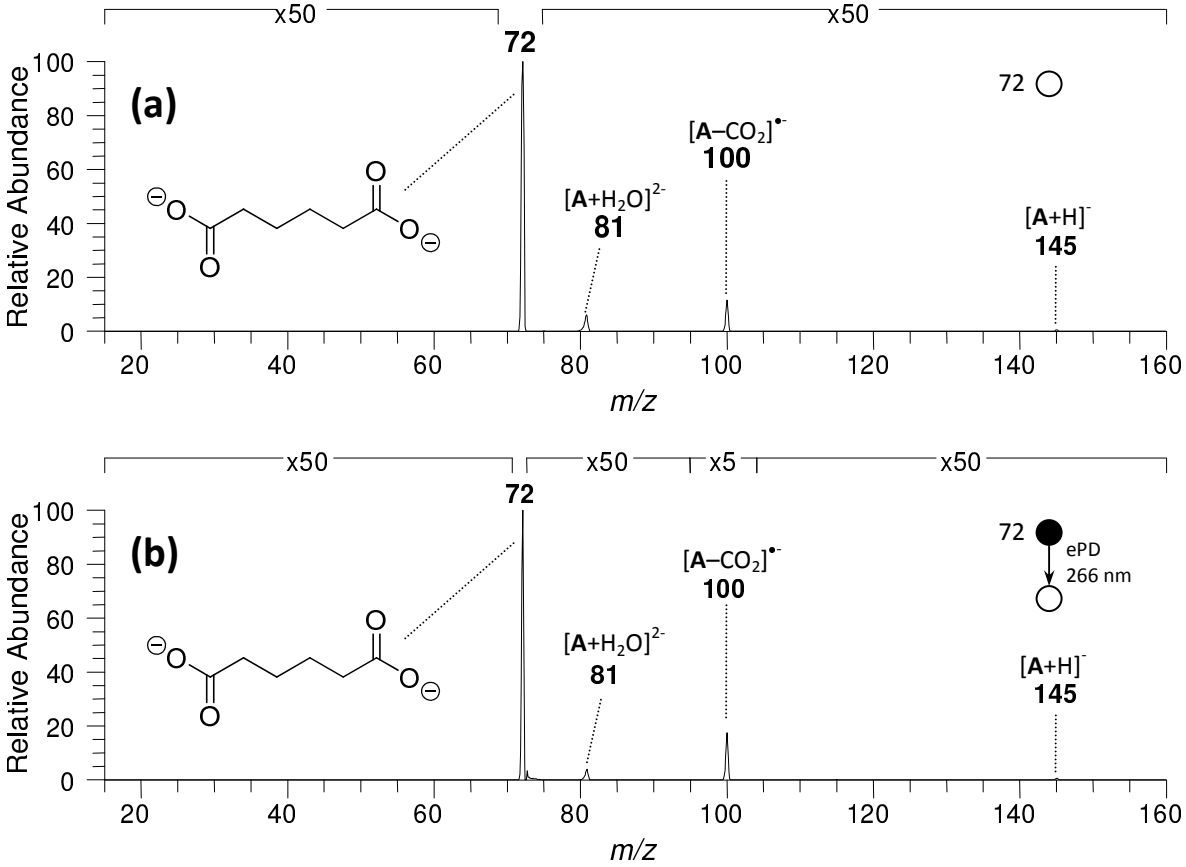

Figure 3: Mass spectrum measured after (a) isolation of the [M - 2H]$^{2-}$ dianion ($\mathbf{A}^{2-}$) at *m/z* 72 formed by ESI of a methanolic solution of adipic acid, and (b) 266 nm electron photodetachment (ePD) of the isolated dianion (*m/z* 72).

(iii) and (iv) are favoured entropically leading to the high abundance of [M + O_2 - HO]$^-$ and [M + O_2 - HO_2]$^-$ at *m/z* 101 and 85, respectively, in the mass spectrum depicted in Figure 2. The combination of two energetically and entropically favourable reaction channels: 1,5-cyclisation to form 1,2-dioxolane + CO_2 + e^-; and 1,5-hydrogen atom transfer and β-scission to form 1-hydroperoxyl-2-propene + CO_2 + e^-, provides a clear rationale for the 39% depletion in the *m/z* 86 ion population not accounted for in the mass spectrum.

3.3. Photodetachment of the [M - 2H]$^{2-}$ dianion of adipic acid ($\mathbf{A}^{2-}$)

The [M - 2H]$^{2-}$ adipate dianion ($\mathbf{A}^{2-}$) at *m/z* 72 was generated by ESI of a methanolic solution of adipic acid. Isolation of the *m/z* 72 dianion resulted in low abundance [**A** + H_2O]$^{2-}$ and [**A** + H]$^-$ ions at *m/z* 81 and 145, respectively (shown in Figure 3a). As

observed during isolation of the glutarate dianion, the $[\mathbf{A} + \mathrm{H}]^-$ ion increases in abundance with longer isolation times, suggesting this ion arises due to proton transfer from either water, methanol or other proton donor present in the ion-trap (see Supporting Information, Figure S4). Subjecting isolated $\mathbf{A}^{2-}$ at *m/z* 72 to 266 nm ePD resulted in a significant enhancement in the yield of the $[\mathbf{A} - \mathrm{CO_2}]^{\bullet-}$ ion at *m/z* 100. There were no other ions of notable abundance identified in the ePD mass spectrum. Importantly, an *m/z* 144 ion corresponding to the adipate radical anion $\mathbf{A}^{\bullet-}$ was not observed, demonstrating the nascent carbonyloxyl radical generated after ePD is not stable on a millisecond timescale, nor are any stable isomers formed. The total ion count measured after ePD of the $\mathbf{A}^{2-}$ at *m/z* 72 decreases by *ca.* 50%, as observed for $\mathbf{G}^{2-}$, suggesting secondary electron detachment, or generation of ions that reside below 25 Th (*i.e.* the low-mass cutoff at *m/z* 72). This is again consistent with the PES experiments of Xing *et al.* where near-zero kinetic electrons were observed after ePD of $\mathbf{A}^{2-}$.

Electronic structure calculations of the putative reaction pathways leading to secondary electron loss channels after initial ePD of the $\mathbf{A}^{2-}$ were performed and the results are described in Scheme 5. δ-Lactonisation of the nascent $\mathbf{A}^{\bullet-}$ carbonyloxyl radical (i) is the lowest energy electron loss channel, with a barrier of only 4.5 kcal mol^{-1} and an overall exothermicity of -7.2 kcal mol^{-1}. 1,6-Hydrogen atom transfer (ii) proceeds over a barrier at 4.7 kcal mol^{-1} to form 1-carboxylato-4-carboxybut-2-yl radical anion with a reaction exothermicity of -28.7 kcal mol^{-1}. The barrier to subsequent β-scission resides at -11.0 kcal mol^{-1} yielding an ion-dipole complex at -15.2 kcal mol^{-1} below $\mathbf{A}^{\bullet-}$ and held together by 17.2 kcal mol^{-1} that releases 1-carboxybutene + $\mathrm{CO_2}$ + $\mathrm{e^-}$ with an overall reaction endothermicity of 2.0 kcal mol^{-1}. Decarboxylation of the nascent carbonyloxyl radical (v) to form 4-carboxylatobutyl radical anion (**4-CB**) is exothermic overall, with the products residing -6.2 kcal mol^{-1} below the precursor. In this case, electron detachment may arise after δ-lactonisation (vi), β-scission reactions (vii), 1,4-cyclisation (viii), or 1,4-hydrogen atom transfer (ix). No transition state was calculated for the lactonisation channel (vi); however, a relaxed scan places the barrier *ca.* 19 kcal mol^{-1} above $\mathbf{A}^{\bullet-}$ to form an intermediate δ-valerolactone radical anion at 2.4 kcal mol^{-1} that promptly emits an electron to form the

neutral lactone with an overall reaction exothermicity of -7.2 kcal mol^{-1}. 1,4-Cyclisation (viii) and 1,4-hydrogen atom transfer (ix) have high barriers residing at 38.3 kcal mol^{-1} and 31.5 kcal mol^{-1}, respectively. 1,4-Cyclisation results in formation of cyclobutane + $CO_2 + e^-$ with an overall reaction exothermicity of -2.4 kcal mol^{-1}, while 1,4-hydrogen atom transfer results in generation of 2-carboxylatobutyl radical anion (**2-CB**) at -10.7 kcal mol^{-1}. The barrier to subsequent β-scission of **2-CB** resides at 2.8 kcal mol^{-1} to generate 1-butene + $CO_2 + e^-$ with a reaction exothermicity of -8.2 kcal mol^{-1}. Alternatively, **4-CB** may undergo β-scission directly with a barrier at 21.3 kcal mol^{-1} to form 2-carboxylatoethyl radical anion + C_2H_4 with a reaction endothermicity of 16.8 kcal mol^{-1}. The barrier to β-scission of 2-carboxylatoethyl radical anion resides at 28.6 kcal mol^{-1} to form $C_2H_4 + CO_2 + e^-$ with an overall reaction endothermicity of 17.6 kcal mol. Each of these reaction pathways, however, contain barriers significantly higher than either direct δ-lactonisation (i) or 1,6-hydrogen atom transfer (ii) of $\mathbf{A}^{\bullet-}$ providing strong evidence to suggest electron detachment arises from direct rearrangment of the nascent $\mathbf{A}^{\bullet-}$ radical anion and not *after* decarboxylation.

Notably, 1,5-hydrogen atom transfer of **4-CB** to form the α-carboxylate isomer, 1-carboxylatobutyl radical anion (**1-CB**), was calculated to require only 14.9 kcal mol^{-1} additional energy corresponding to a barrier of 21.1 kcal mol^{-1} with respect to **4-CB**. This is substantially less energy than the 35.4 kcal mol^{-1} predicted for the analogous 1,4-hydrogen atom transfer of **3-CP** to form **1-CP**. Furthermore, this barrier is 9.8 and 10.8 kcal mol^{-1} lower than both 1,3- and 1,4-hydrogen atom transfer resulting in the 2-carboxylatobutyl (**2-CB**) and 3-carboxylatobutyl (**3-CB**) radical anions, respectively. It was not possible to distinguish between the dianion and the β-scission product 2-carboxylatoethyl radical anion, as the parent and product are isobaric; however, the barrier for this process is 6.4 kcal mol^{-1} higher than 1,5-hydrogen atom transfer.

In order to test for isomerisation of the nascent **4-CB** to **1-CB**, the m/z 100 ion was isolated in the presence of background O_2 and the resulting mass spectrum is shown in Figure 5(a). The natural logorithm of the m/z 100 ion decay plotted against isolation time was non-linear, suggesting that there are multiple isomers with different rate constants present in the ion population. Furthermore, the total ion count decreased by 82% after isolating

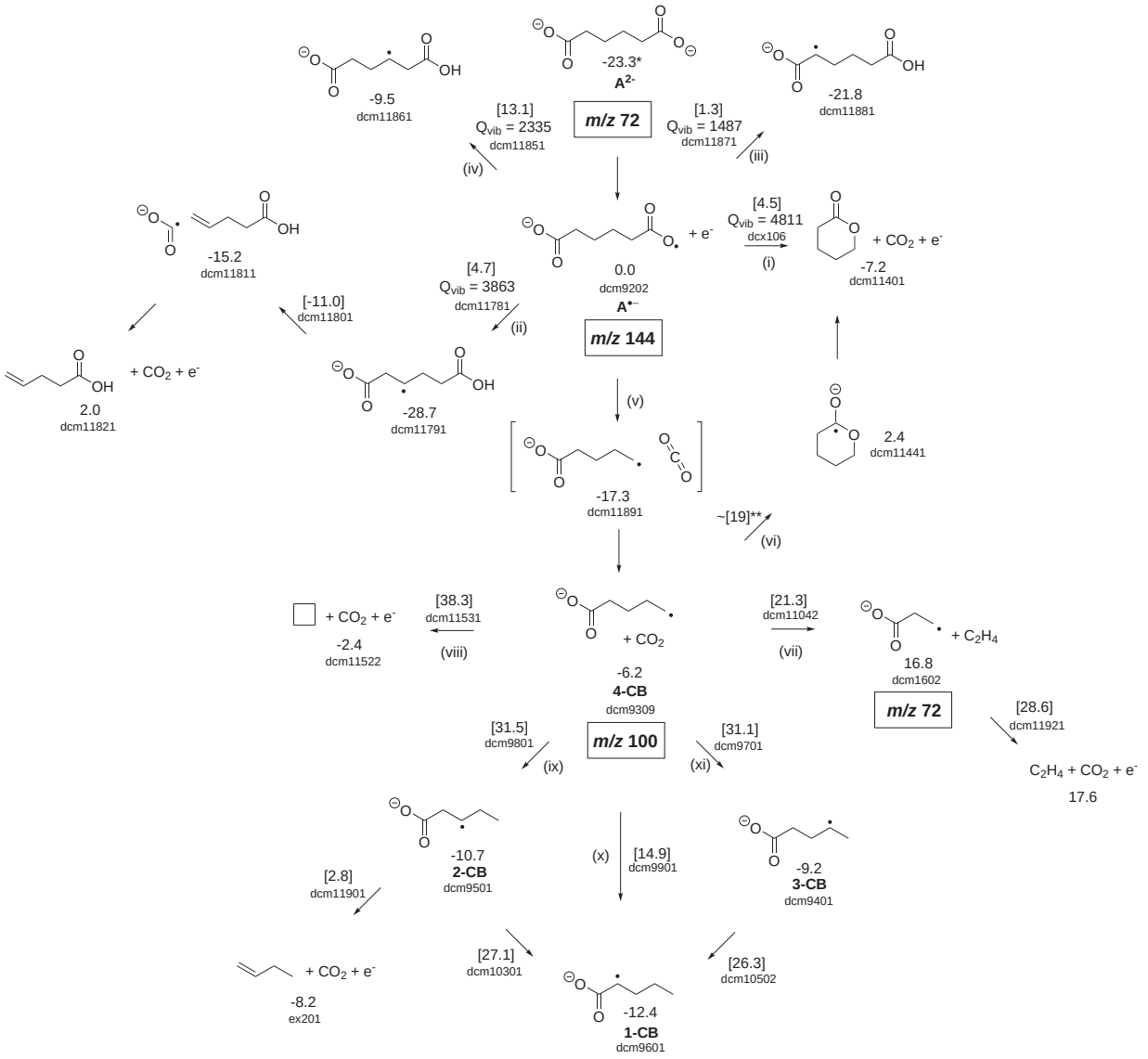

Scheme 5: Potential fragmentation pathways of the adipate dianion. Energies were calculated at the M06-2X/6-311++G(d,p) level and include unscaled zero-point energy corrections. Energies are reported relative to $\mathbf{A}^{\bullet-}$ and include all neutral fragments along the reaction channel (*i.e.*, the energy of the initial carbon dioxide is included). The codes provided beneath each structure are references to the raw geometry and energy data reported in Supporting Information. * Energy was calculated from the electron binding energy measured by Wang *et al.* [46]. ** Energy estimated from a relaxed potential energy scan (see Supporting Information, Figure S8) and does not include zero-point energy correction.

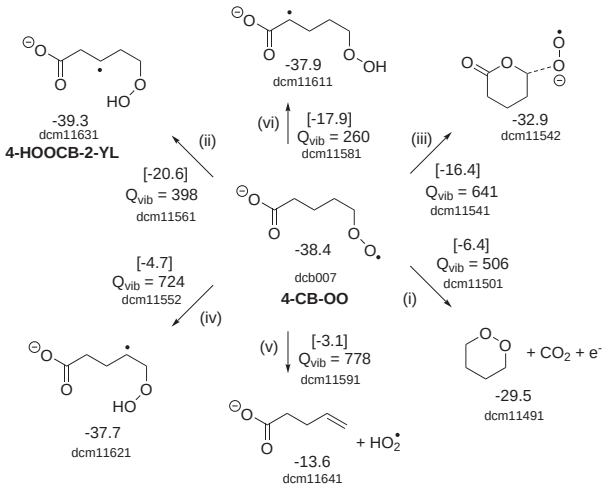

Scheme 6: Potential reaction pathways of the 4-carboxylatobutylperoxyl radical anion with estimated vibrational partition functions (Q_{vib}). Calculated at the M06-2X/6-311++G(d,p) level. Energies are provided relative to the 4-carboxylatobutyl radical anion (**4-CB**) + O_2 entrance channel and include unscaled zero-point energy corrections. The codes provided beneath each structure are references to the raw geometry and energy data reported in Supporting Information.

the m/z 100 ion in the presence of O_2 for 5000 ms, suggesting a significant proportion of product ions reside below the low-mass cutoff (50 Th in these experiments) or are accessing product channels that involve electron detachment. Dominant ions arose at m/z 60, 99 and 115, assigned as $CO_3^{\bullet-}$, $[M + O_2 - HO_2]^-$ and $[M + O_2 - HO]^-$ ions, respectively. The presence of $CO_3^{\bullet-}$ at m/z 60 demonstrates that some proportion of the ion population at m/z 100 has rearranged to the more energetically stable α-carboxylate isomer **1-CB**. $[M - 13]^-$, $[M\text{-}15]^-$, $[M\text{-}27]^-$, $[M - 29]^-$ ions arise at m/z 87, 85, 73 and 71 and were assigned as addition of O_2 followed by subsequent ejection of $HO + CO$, $HO + CH_2O$, $HO + C_2H_2O$ and $HO + CO_2$, respectively. The observation of $[M + O_2 - HO_2]^-$, $[M + O_2 - HO]^-$, in addition to the ions just identified, suggests a significant quantity of distonic carboxylatobutyl radical anion(s) (**2-CB**, **3-CB** or **4-CB**) remain in the m/z 100 precursor ion population.

To investigate whether the additional products may be formed from **1-CB**, an independent synthesis of this isomer was developed. As described in Scheme 8, 2-iodovalerate anion was subjected to photodissociation (266 nm) to yield **1-CB** at m/z 100 (Figure 4). Isolation of **1-CB** in the presence of O_2 resulted in the spectrum depicted in Figure 5(b). The major

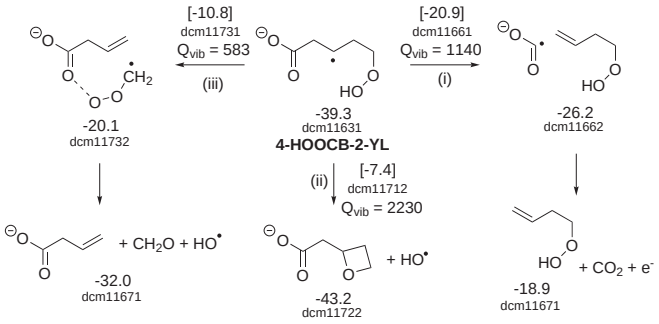

Scheme 7: Potential fragmentation pathways of the 1-carboxylato-4-hydroperoxylbut-2-yl radical anion with estimated vibrational partition functions (Q_{vib}). Energies were calculated at the M06-2X/6-311++G(d,p) level and include unscaled zero-point energy corrections. The codes provided beneath each structure are references to the raw geometry and energy data reported in Supporting Information.

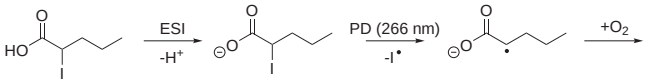

Scheme 8: Reaction scheme for generation of authentic 1-carboxylatobutyl radical anion by photodissociation of 2-iodovalerate anion generated by ESI of 2-iodovaleric acid.

ion in this spectrum arises at m/z 60, assigned as $CO_3^{\bullet-}$, consistent with previous reports of α-carboxylate reactivity towards O_2 [37]. Interestingly, the total ion count did not decrease over increasing isolation time indicating that no electron loss channels arise during reaction of **1-CB** with O_2. An $[M - 1]^-$ ion is featured at m/z 99; however, this ion is present during the initial isolation of the m/z 100 ion (*i.e.* isolation time of 0.03 ms), which requires a large isolation width and furthermore, does not increase in abundance over increased trapping time. Therefore, the m/z 99 ion is assigned as arising due to loss of HI from the parent 2-iodovalerate ion and not due to reaction of **1-CB** with O_2. As such, the only ion arising from reaction with O_2 is $CO_3^{\bullet-}$ at m/z 60.

To account for the significant decrease in total ion count after reaction of **4-CB** with O_2, we allowed the product ions generated after ePD of $\mathbf{A}^{2-}$ (m/z 72) to react with O_2, without secondary isolation of the carboxylatobutyl radical anion (m/z 100) photoproduct. This allows us to decrease the low-mass cutoff to 25 Th. After subtracting the spectrum measured when the dianion is isolated without ePD (presented in Supporting Information, Figure S4 and S5), $O_2^{\bullet-}$ at m/z 32 ion was observed with an abundance only 10% lower

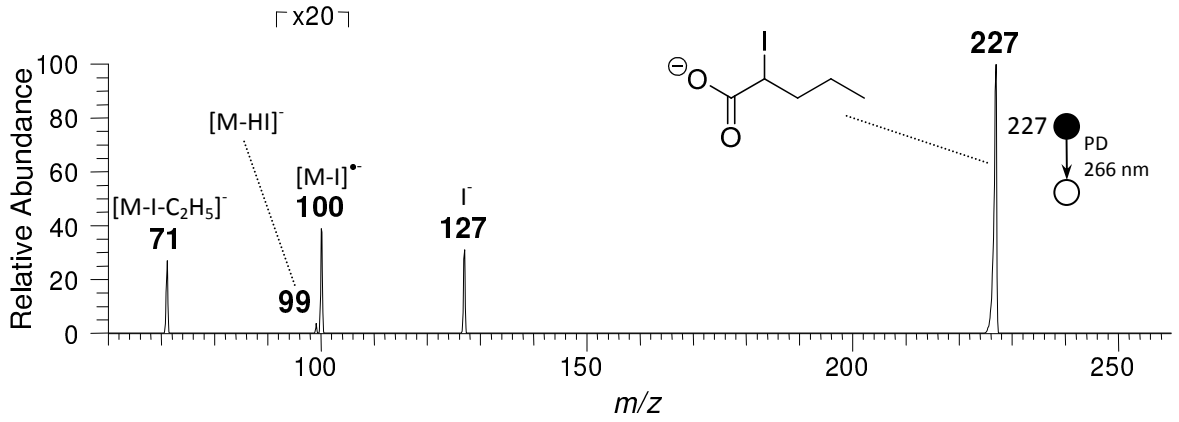

Figure 4: Mass spectrum measured after 266 nm photodissociation of 2-iodovalerate (m/z 227)

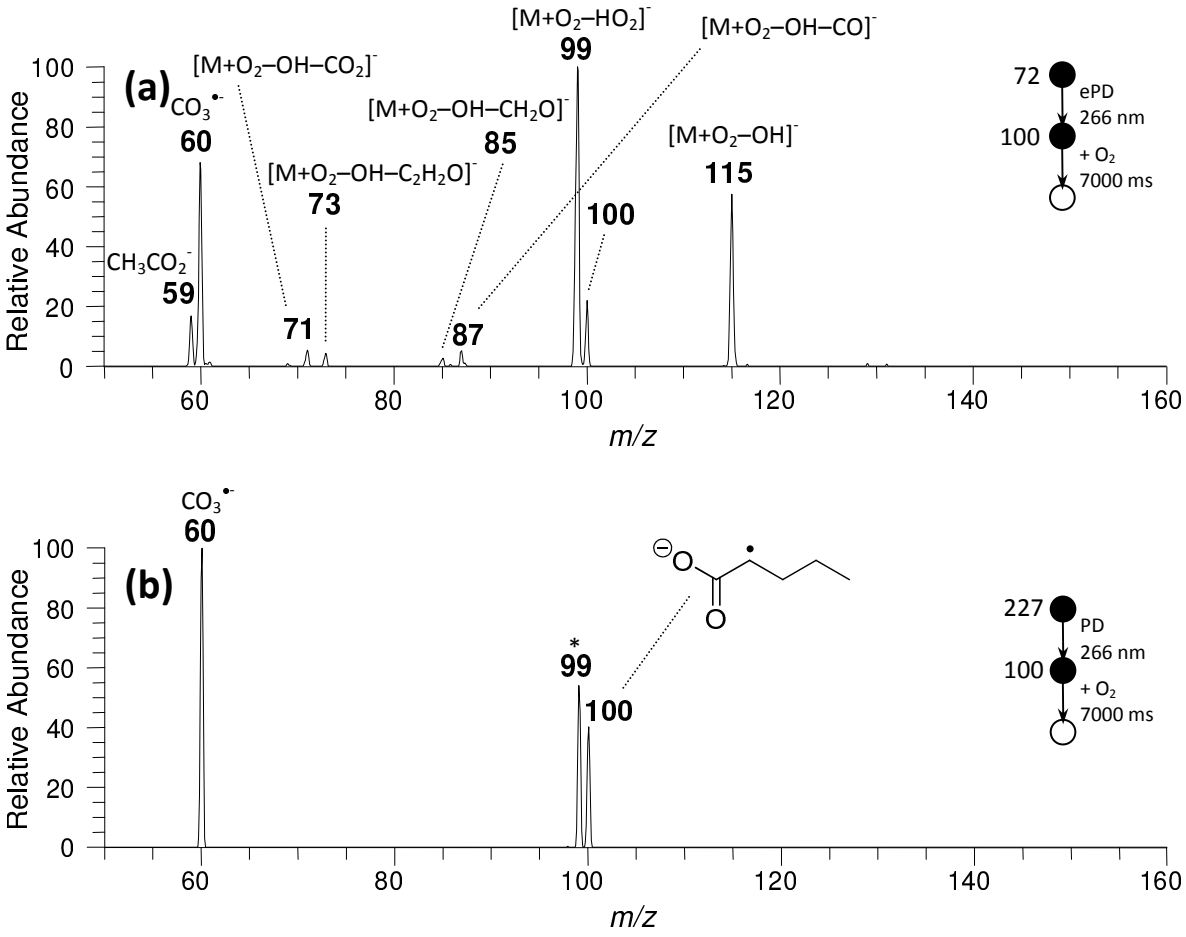

Figure 5: Mass spectrum measured after reaction of the (a) [**A** - CO_2]$^{\bullet-}$ ion at m/z 100 generated after ePD of the adipate dianion (**A**$^{2-}$, m/z 72), and (b) genuine 1-carboxylatobutyl radical anion (m/z 100) generated by PD of 2-iodovaleric acid with O_2 for 7000 ms. * This ion arises due to loss of HI from the precursor 2-iodovalerate and not due to reaction of the 1-carboxylatobutyl radical anion (m/z 100) with O_2.

than $CO_3^{\bullet-}$ at m/z 60. However, this ion accounts for only 2% of the lost total ion count and there is therefore still an 80% loss of the precursor ion signal that connot be accounted for by detectable product ions.

Analogous to the pathways described for **3-CP-OO**, we have calculated two alternative channels that result in electron loss during rearrangement of **4-CB-OO** (Scheme 6): cyclisation to form a cyclic peroxide (i) and 1,6-hydrogen atom transfer with concomitant β-scission (ii). The 1,6-cyclisation pathway (i) requires 32.0 kcal mol^{-1} to form 1,2-dioxane + CO_2 + e^- with the products residing -29.5 kcal mol^{-1} below the entrance channel. Analysis of the vibrational partition functions (Q_{vib}) however, suggests that this channel is entropically disfavoured over δ-lactonisation (iii) or 1,5-hydrogen atom transfer (iv and v) and its barrier is significantly higher than both 1,6- and 1,7-hydrogen atom transfers (pathways ii and vi, respectively). 1,6-Hydrogen atom transfer (ii) is the lowest energy reaction channel with a barrier at -20.6 kcal mol^{-1} resulting in formation of 4-hydroperoxyl-1-carboxylato-2-butyl radical anion (**4-HOOCB-2-YL**) with an exothermicity of -39.3 kcal mol^{-1}. As described in Scheme 7, the lowest energy reaction pathway subsequent to formation of **4-HOOCB-2-YL** is β-scission to generate 3-hydroperoxylbutene + CO_2 + e^-, which proceeds over a barrier residing at -20.9 kcal mol^{-1} to from an ion-dipole complex at -26.2 kcal mol^{-1} releasing the products with a reaction exothermicity of -18.9 kcal mol^{-1}. Overall, these calculations suggest 1,6-hydrogen atom transfer with concomitant β-scission to generate 3-hydroperoxylbutene is the most favourable electron detachment pathway accessible from reaction of **4-CB** with O_2.

4. Discussion

We have generated two short-chain aliphatic dicarboxylate dianions, glutarate ($\mathbf{G}^{2-}$) and adipate ($\mathbf{A}^{2-}$) dianion, and subjected both to 266 nm laser ePD in an ion-trap mass spectrometer. A significant abundance of the total ion count was lost in each case, indicating product branching includes electron loss channels to form neutral molecules or generation of product ions residing below the low-mass cutoff that are not detected by mass spectrometry. It is unlikely that we have generated ions lower than the low-mass cutoff; therefore, we

expect that the total ion count loss is predominantly due to secondary electron detachment consistent with the PES measurements of Xing *et al.* [20]. An energetically competitive lactonisation pathway was calculated for both the glutarate ($\mathbf{G}^{\bullet-}$) and adipate ($\mathbf{A}^{\bullet-}$) radical anions with barriers of only 5.4 kcal mol^{-1} and 4.5 kcal mol^{-1} (Schemes 2ix and 5i), respectively. The nascent $\mathbf{G}^{\bullet-}$ and $\mathbf{A}^{\bullet-}$ radical anions may also undergo hydrogen atom transfers with similar barriers of only 5.1 kcal mol^{-1} and 4.7 kcal mol^{-1}, respectively, to form intermediates that release $CO_2 + e^-$ after β-scission (Schemes 2viii and 5ii). Interestingly, the intrinsic reaction coordinates calculated for both lactonisation and hydrogen transfer transition states suggest decarboxylation directly intersects these reaction pathways (see Supporting Information, Figure S7). Furthermore, the two respective 1,6- and 1,7-hydrogen atom transfers for $\mathbf{G}^{\bullet-}$ and $\mathbf{A}^{\bullet-}$ that result in stable cross-conjugated α-carboxylate radical anions (Schemes 2x and 5iii for $\mathbf{G}^{\bullet-}$ and $\mathbf{A}^{\bullet-}$, respectively) are the least entropically favoured pathways predicted by their relative Q_{vib} values. This explains why we may not see stable [M - 2H]$^{\bullet-}$ ions at *m/z* 130 or *m/z* 144 arising from rearrangement to stable isomers. In contrast, should $\mathbf{G}^{\bullet-}$ and $\mathbf{A}^{\bullet-}$ promptly decarboxylate after ePD, β-scission, cyclisation and hydrogen atom transfer driven electron detachment pathways require signifantly more energy (Schemes 2 and 5). Our ability to isolate the [M - 2H - CO_2]$^{\bullet-}$ radical anion generated in each case for a number of seconds provides strong evidence that these radical anions are stable with respect to electron detachment. Taken together, these experimental and theoretical results suggest secondary electron detachment occurs by direct rearrangement of the nascent $\mathbf{G}^{\bullet-}$ and $\mathbf{A}^{\bullet-}$ radical anions and not after prompt decarboxylation as previously proposed (Scheme 1) [20].

Photoelectron spectra of $\mathbf{G}^{2-}$ and $\mathbf{A}^{2-}$ previously reported by Xing *et al.* suggest that after 266 nm ePD the nascent carbonyloxyl radicals generated may have up to *ca.* 1.4 eV (32.3 kcal mol^{-1}) and 1.2 eV (27.7 kcal mol^{-1}) vibronic excitation energy, respectively. In the case of $\mathbf{G}^{\bullet-}$ radical anion, decarboxylation resulting in the formation of **3-CP** with a reaction energy of -2.5 kcal mol^{-1} provides a maximum of 34.8 kcal mol^{-1} of vibrational energy. There is, therefore, insufficient energy for 1,3-cyclisation and only very small populations of ions will contain sufficient energy for either 1,3- or 1,4-hydrogen atom transfer. In

comparison, γ-lactonisation resulting in electron autodetachment requires 31.7 kcal mol^{-1}, while the β-scission reaction channel generating acetate radical anion contains a barrier of 29.2 kcal mol^{-1}. Acetate radical anion was detected only in small quantities (see Figure 1b), suggesting γ-lactonisation of **3-CP** likely occurs to an even lesser extent. Taken together, these data suggest the major decarboxylated product generated was **3-CP** and it is unlikely that this product releases secondary electrons. Similarly, after decarboxylation of the $\mathbf{A}^{\bullet-}$ radical anion, *ca.* 33.9 kcal mol^{-1} of vibronic excitation energy is available for isomerisation of **4-CB**. There is insufficient energy for 1,3-cylisation and only small populations of ions will have the required energy for 1,3- and 1,4-hydrogen atom transfer. A barrier for δ-lactionisation that results in electron autodetachment was estimated at *ca.* 19 kcal mol^{-1} with respect to $\mathbf{A}^{\bullet-}$ residing well within the energy available; however, the lowest energy pathway is 1,5-hydrogen atom transfer with a barrier residing at only 14.9 kcal mol^{-1}, suggesting this pathway will be be favourble to form **1-CB**.

The diagnostic reaction of alkyl carboxylates with O_2 was used to confirm the identity of both the propyl and butyl carboxylate radical anions generated by decarboxylation of the nascent [M - 2H]$^{\bullet-}$ carbonyloxyl radicals formed after ePD of $\mathbf{G}^{2-}$ and $\mathbf{A}^{2-}$ dianions. Reaction of the [**G** - CO_2]$^{\bullet-}$ propyl carboxylate radical anion population resulted in no carbonate radical anion ($CO_3^{\bullet-}$) at *m/z* 60, confirming **3-CP** does not isomerise to the lowest energy **1-CP** radical anion. 1,4-Hydrogen atom transfer of **3-CP** resulting in formation of **1-CP** requires 1.9 kcal mol^{-1} less energy than 1,3-hydrogen atom transfer to form **2-CP**, suggesting that **2-CP** is not generated during decarboxylation of the glutarate radical anion and the only isomer present in the decarboxylated ion population is **3-CP** (Scheme 2). In contrast, reaction of the [**A** - CO_2]$^{\bullet-}$ butyl carboxylate radical anion population results in formation of abundant $CO_3^{\bullet-}$ at *m/z* 60 (see Figure 5a). In this case, *m/z* 60 accounted for *ca.* 20% of the isolated ionic products. An approximation of the contribution of **1-CB** isomers to the *m/z* 100 ion population may be made by considering the reaction of authentic **1-CB**, generated by PD of 2-iodovalerate anion, with O_2. This reaction resulted exclusively in formation of $CO_3^{\bullet-}$ and importantly, the total ion count did not decrease at longer reaction times, indicating there are no reaction channels resulting in low-mass ions or electron

autodetachment. As such, the 80% decrease in total ion count must arise due to reaction of one of the distonic isomers and not **1-CB**. Therefore, **1-CB** can account for only 3% of the total butyl carboxylate radical anion population. The barriers to 1,5- and 1,6-hydrogen atom transfer of **4-CB** are higher than the highest vibronic excitation energy measured by Xing *et al.* [20], which suggests the remaining 97% of the carboxylatobutyl radical anion population generated after decarboxylation of the nascent adipate radical anion is **4-CB**.

The most likely explanation for the ion loss observed during reaction of **3-CP** and **4-CB** with O_2 is competitive β-scission reactions after hydrogen atom transfer generates a β-carboxylate radical. For example, **3-CP-OO** may undergo β-scission after 1,5-hydrogen atom transfer of **3-HOOCP-2-YL** to release $CO_2 + e^-$ (Scheme 3). This process is energetically favourable over both ejection of HO and HO_2 with a barrier of 11.8 kcal mol^{-1} compared with barriers of 23.3 kcal mol^{-1} and 22.7 kcal mol^{-1}, respectively. However, this β-scission channel will likely compete entropically with HO_2 loss, as indicated by their relative Q_{vib} parameters (depicted in Scheme 4). Furthermore, while 1,5-hydrogen atom transfer is entropically favourable, the barrier to 1,5-hydrogen atom transfer is higher than both 1,6-hydrogen atom transfer and γ-lactonisation. In contrast, 1,6-hydrogen atom transfer of **4-CB-OO** resulting in **4-HOOCB-2-YL** is the lowest energy reaction pathway. This intermediate may eject $CO_2 + e^-$ after β-scission, requiring 18.4 kcal mol^{-1} to overcome the barrier to form an ion-dipole complex -26.2 kcal mol^{-1} below the entrance channel. This ion-dipole complex is held together by 7.3 kcal mol^{-1} and releases the products 1-hydroperoxylbut-3-ene + $CO_2 + e^-$ with a reaction exothermicity of -18.9 kcal mol^{-1}. Importantly, β-scission to release $CO_2 + e^-$ from the **4-HOOCB-2-YL** is both energetically and entropically favoured over the alternative β-scission to eject CH_2O + HO, or epoxidation generating HO. Taken together, the difference in total ion count loss can be explained by considering formation of **3-HOOCP-2-YL** is not the lowest energy pathway and after its generation and must compete with HO and HO_2 ejection, whereas formation of **4-HOOCB-2-YL** and subsequent β-scission and ejection of $CO_2 + e^-$ is overall the lowest energy reaction channel and is both energetically and entropically favourable.

5. Conclusion

We have identified low-energy hydrogen atom transfer and lactonisation pathways can facilitate secondary electron detachment directly from $[O_2C{-}(CH_2)_n{-}CO_2]^{\bullet-}$ carbonyloxyl radical anions. These reaction pathways are illustrated in a general form in Scheme 9 and can account for the loss of ion signal observed following ePD of glutarate and adipate dianions in the ion-trap mass spectrometer. Similarly, these pathways most likely account for the detection of near-zero kinetic energy electrons observed in the PES studies of the same dianions by Wang and co-workers [20]. Importantly our results indicate that these rearrangement pathways of the radical anion intermediate (resulting in electron autodetachment) compete kinetically with decarboxylation. Competition between decarboxylation and intramolecular rearrangement has previously been observed; Schröder *et al.* found long-chained alkylcarbonyloxyl radicals ($n \geq 5$) had a lifetime sufficient during neutralisation-reionisation experiments to undergo hydrogen atom transfers prior to reionisation [26]. Similarly, while this phenomenon is not discussed in their investigation, Joly *et al.* measured stable $[M - 2H]^{\bullet-}$ radical anions following ePD of $[M - 2H]^{2-}$ dianions formed from peptides [51, 52]. In all likelihood, such ions are stable isomers resulting from rearrangement of the nascent radical anion: a process that again competes favourably with prompt decarboxylation. These observations from our own work and that of others suggest that ePD of dicarboxylate dianions may in the future provide an interesting laboratory within which to explore the chemistry

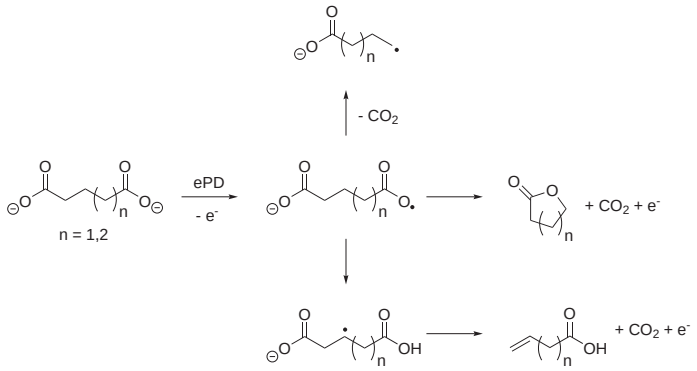

Scheme 9: Putative fragmentation pathways of dicarboxylate dianions after electron photodetachment resulting in secondary electron detachment.

of carbonyloxyl radicals that have proved somewhat elusive to the experimentalist.

6. Acknowledgements

The authors acknowledge the financial support of the Australian Research Council (DP0986738, DP120102922, DE120100467) and the University of Wollongong. S.J.B., A.J.T. and B.B.K. acknowledge the support of the ARC Centre of Excellence for Free Radical Chemistry and Biotechnology (CE0561607) and for a generous allocation of computational resources by the University of Wollongong (NSW, Australia), in addition to Intersect (NSW, Australia) and the NCI National Facility (Canberra, Australia) under Merit Allocation Schemes. The authors would like to thank Nicholas D. Reed, Celli Lloyd and Pramesh I. Hettiarachachi for help with related experiments. S.J.B. would like to acknowledge the helpful insights provided by Detlef Schröder following the initial presentation of our results at ASMS60 in Vancouver. Detlef's generosity in sharing his passion for, and extraordinary insight into, the chemistry of gas phase ions was an inspiration that will be sorely missed.

References

[1] X.-B. Wang, L.-S. Wang, Photoelectron spectroscopy of multiply charged anions, Ann. Rev. Phys. Chem. 60 (2009) 105–126.

[2] M. K. Scheller, R. N. Compton, L. S. Cederbaum, Gas-phase multiply charged anions, Science 270 (1995) 1160–1166.

[3] W. K. Stuckey, R. W. Kiser, Doubly charged negative ions of oxygen, fluorine, chlorine and bromine, Nature 211 (5052) (1966) 963–964.

[4] J. H. Fremlin, Doubly charged negative ions, Nature 212 (5069) (1966) 1453.

[5] H. Baumann, E. Heinicke, H. J. Kaiser, K. Bethge, On the existence of doubly negative charged heavy ions, Nucl. Instrum. Meth. 95 (2) (1971) 389–391.

[6] J. E. Ahnell, W. S. Koski, Evidence for doubly charged negative fluorine ions from electorn bombardment of CF_3Cl, Nature Physical Science 245 (1973) 30–31.

[7] D. Spence, W. A. Chupka, C. M. Stevens, Search for long-lived doubly charged atomic negative ions, Phys. Rev. A 26 (1) (1982) 654–657.

[8] K. H. Chang, R. D. McKeown, R. G. Milner, J. Labrenz, Search for long-lived doubly charged negative atomic ions, Phys. Rev. A 35 (9) (1987) 3949–3951.

[9] L. Frees, E. Heinicke, W. S. Koski, Concerning double charged negative ions of iodine in the gas phase, Nucl. Instrum. Meth. 159 (1) (1979) 105–107.

[10] J. H. Bowie, B. J. Stapleton, Electron impact studies. c. doubly charged negative ions, J. Am. Chem. Soc. 98 (21) (1976) 6480.

[11] S. N. Schauer, P. Williams, R. N. Compton, Production of small doubly charged negative carbon cluster ions by sputtering, Phys. Rev. Lett. 65 (5) (1990) 625–628.

[12] R. L. Hettich, R. N. Compton, R. H. Ritchie, Doubly charged negative ions of carbon-60, Phys. Rev. Lett. 67 (10) (1991) 1242–1245.

[13] R. N. Compton, A. A. Tuinman, C. E. Klots, M. R. Pederson, D. C. Patton, Electron attachment to a negative ion: $e + C_{84}^{-} \rightleftharpoons C_{84}^{-2}$, Phys. Rev. Lett. 78 (23) (1997) 4367–4370.

[14] J. B. Fenn, M. Mann, C. K. Meng, S. F. Wong, C. M. Whitehouse, Electrospray ionization for mass spectrometry of large biomolecules, Science 246 (1989) 64–71.

[15] J. A. Loo, R. R. Ogorzalek Loo, K. J. Light, C. G. Edmonds, R. D. Smith, Multiply charged negative ions by electrospray ionization of polypeptides and proteins, Anal. Chem. 64 (1992) 81–88.

[16] J. L. Beck, M. L. Colgrave, S. F. Ralph, M. M. Sheil, Electrospray ionization mass spectrometry of oligonucleotide complexes with drugs, metals and proteins, Mass Spectrom. Rev. 20 (2) (2001) 61–87.

[17] F. Hsu, J. Turk, E. R. Rhoades, D. G. Russell, Y. Shi, E. A. Groisman, Structural characterization of cardiolipin by tandem quadrupole and multiple-stage quadrupole ion-trap mass spectrometry with electrospray ionization, J. Am. Soc. Mass Spectrom. 16 (2004) 491–504.

[18] L.-S. Wang, C.-F. Ding, X.-B. Wang, J. B. Nicholas, Probing the potential barriers and intramolecular electrostatic interactions in free doubly charged anions, Phys. Rev. Lett. 81 (13) (1998) 2667–2670.

[19] C. F. Ding, X. B. Wang, L. S. Wang, Photoelectron spectroscopy of double charged anions: Intramolecular coulomb repulsion and solvent stabilization, J. Phys. Chem. A 102 (45) (1998) 8633–8636.

[20] X.-P. Xing, X.-B. Wang, L.-S. Wang, Photoelectron imaging of double charged anions, $^{-}O_2C(CH_2)_nCO_2^{-}$ (n = 2-8): Observation of near 0 eV electrons due to secondary dissociative autodetachment, J. Phys. Chem. A 114 (2010) 4524–4530.

[21] P. Skurski, J. Simons, X. B. Wang, L. S. Wang, Experimental and theoretical investigations of the stability of two small gaseous dicarboxylate dianions: Acetylene dicarboxylate and succinate, J. Am. Chem. Soc. 122 (2000) 4499–4507.

[22] Z. Lu, R. E. Continetti, Dynamics of the acetyloxyl radical studied by dissociative photodetachment of the acetate anion, J. Phys. Chem. A 108 (2004) 9962–9969.

[23] S. Yamauchi, N. Hirota, S. Takahara, H. Misawa, K. Sawabe, H. Sakuragi, K. Tokumaru, A time-resolved epr study on photodecomposition of dibenzoyl peroxides in carbon tetrachloride, J. Am. Chem. Soc. 111 (1989) 4402–4407.

[24] W. Braun, L. Rajbenbach, F. R. Eirich, Peroxide decomposition and cage effect, J. Phys. Chem. 66 (9) (1962) 1591–1595.

[25] B. Abel, J. Assmann, M. Buback, C. Grimm, M. Kling, S. Schmatz, J. Schroeder, T. Witte, Ultrafast decarboxylation of carbonyloxy radicals: Influence of molecular structure, J. Phys. Chem. A 107 (2003) 9499–9510.

[26] D. Schröder, H. Soldi-Lose, H. Schwarz, Unimolecular rearrangements of transient carboxy radicals and cations, Aust. J. Chem. 56 (5) (2003) 443–451.

[27] T. Tabarin, R. Antoine, M. Broyer, P. Dugourd, Specific photodissociation of peptides with multi-stage mass spectrometry, Rapid Commun. Mass Spectrom. 19 (20) (2005) 2883–2892.

[28] F. O. Talbot, T. Tabarin, R. Antoine, M. Broyer, P. Dugourd, Photodissociation spectroscopy of trapped protonated tryptophan, J. Chem. Phys. 122 (2005) 074310.

[29] B. B. Kirk, A. J. Trevitt, S. J. Blanksby, Does addition of NO_2 to carbon-centered radicals yield RONO or RNO_2? an investigation using distonic radical ions, J. Am. Chem. Soc. 24 (2013) 481–492.

[30] C. S. Hansen, B. B. Kirk, S. J. Blanksby, R. A. J. O'Hair, A. J. Trevitt, UV photodissociation action spectroscopy of haloanilinium ions in a linear quadrupole ion trap mass spectrometer, J. Am. Soc. Mass Spectrom. 24 (2013) 932–940.

[31] A. T. Maccarone, B. B. Kirk, C. S. Hansen, T. M. Griffiths, S. Olsen, A. J. Trevitt, S. J. Blanksby, Direct observation of photodissociation products from phenylperoxyl radicals isolated in the gas phase, J. Am. Chem. Soc. DOI:10.1021/ja402610s.

[32] H. Finkelstein, Preparation of organic iodides from the corresponding bromides and chlorides., Ber. 43 (1910) 1528–1532.

[33] J. C. Schwartz, M. W. Senko, J. E. P. Syka, A two-dimensional quadrupole ion trap mass spectrometer, J. Am. Soc. Mass Spectrom. 13 (2002) 659–669.

[34] D. G. Harman, S. J. Blanksby, Investigation of the gas phase reactivity of the 1-adamantyl radical using a distonic radical anion approach, Org. Biomol. Chem. 5 (2007) 3495–3503.

[35] T. Ly, R. R. Julian, Residue-specific radical-directed dissociation of whole proteins in the gas phase, J. Am. Chem. Soc. 130 (2008) 351–358.

[36] T.-Y. Kim, M. S. Thompson, J. P. Reilly, Peptide photodissociation at 157nm in a linear ion trap mass spectrometer, Rapid Commun. Mass Spectrom. 19 (2005) 1657–1665.

[37] T. Ly, B. B. Kirk, P. I. Hettiarachchi, B. L. J. Poad, A. J. Trevitt, G. da Silva, S. J. Blanksby, Reactions of simple and peptidic alpha-carboxylate radical anions with dioxygen in the gas phase, Phys. Chem. Chem. Phys. 13 (2011) 16314–16323.

[38] B. L. J. Poad, B. B. Kirk, P. I. Hettiarachchi, A. J. Trevitt, S. J. Blanksby, T. Clark, Direct observation of a stable carbonyloxyl radical in the gas phase, Angew. Chem. Int. Ed. DOI:10.1002/anie.201304316

(2013) Accepted.

[39] M. J. Frisch, G. W. Trucks, H. B. Schlegel, G. E. Scuseria, M. A. Robb, J. R. Cheeseman, G. Scalmani, V. Barone, B. Mennucci, G. A. Petersson, H. Nakatsuji, Y. Honda, O. Kitao, H. Nakai, T. Vreven, J. A. Montgomery, Jr., J. E. Peralta, F. Ogliaro, M. Bearpark, J. J. Heyd, E. Brothers, K. N. Kudin, V. N. Staroverov, T. Keith, R. Kobayashi, J. Normand, K. Raghavachari, A. Rendell, J. C. Burant, S. S. Iyengar, J. Tomasi, M. Cossi, N. Rega, J. M. Millam, M. Klene, J. E. Knox, J. B. Cross, V. Bakken, C. Adamo, J. Jaramillo, R. Gomperts, R. E. Stratmann, O. Yazyev, A. J. Austin, R. Cammi, C. Pomelli, J. W. Ochterski, R. L. Martin, K. Morokuma, V. G. Zakrzewski, G. A. Voth, P. Salvador, J. J. Dannenberg, S. Dapprich, A. D. Daniels, O. Farkas, J. B. Foresman, J. V. Ortiz, J. Cioslowski, D. J. Fox, Gaussian 09 (2010).

[40] J. M. Hevko, S. Dua, J. H. Bowie, M. S. Taylor, Gas phase and condensed phase sni reactions. the competitive six and seven centre cyclisations of the 5,6-epoxyhexoxide anion. a joint experimental and ab initio study. a comparison with SN_i reactions of homologous epoxyalkoxide anions, J. Chem. Soc., Perkin Trans. 2 (1999) 457–464.

[41] A. M. McAnoy, S. Dua, S. J. Blanksby, J. H. Bowie, The loss of CO from the *ortho*, *meta* and *para* forms of deprotonated methyl benzoate in the gas phase, J. Chem. Soc., Perkin Trans. 2 (2000) 1665–1673.

[42] A. M. McAnoy, M. R. L. Paine, S. J. Blanksby, Reactions of the hydroperoxide anion with dimethyl methylphosphonate in an ion trap mass spectrometer: evidence for a gas phase α-effect, Org. Biomol. Chem. 6 (2008) 2316–2326.

[43] P. W. Atkins, J. de Paula, Physical Chemistry, 9th Edition, Oxford University Press, Oxford, 2010.

[44] K. W. M. Siu, G. J. Gardner, S. S. Berman, Multiply charged ions in ionspray tandem mass spectrometry, Org. Mass. Spectrom. 24 (1989) 931–942.

[45] S. R. Kass, K. M. Broadus, Reactive intermediates via Fourier transform mass spectrometry, J. Phys. Org. Chem. 15 (8) (2002) 461–468.

[46] X. B. Wang, C. F. Ding, L.-S. Wang, Electron tunneling through the repulse coulomb barrier in photodetachment of multply charged anions, Chem. Phys. Lett. 307 (1999) 391–396.

[47] S. J. Yu, C. L. Holliman, D. L. Rempel, M. L. Gross, The β-distonic ion from the reaction of pyridine radical cation and ethene: A demonstration of high-pressure trapping in fourier transform mass spectrometry, J. Am. Chem. Soc. 115 (1993) 9676–9682.

[48] A. E. P. M. Sorrilha, F. C. Gozzo, R. S. Pimpim, M. N. Eberlin, Multistage pentaquadrupole mass spectrometry for generation and characterization of gas-phase ionic species. the case of the $PyC_2H_5^{+\cdot}$ isomers, J. Am. Soc. Mass. Spectrom. 7 (1996) 1126–1137.

[49] B. B. Kirk, D. G. Harman, S. J. Blanksby, Direct observation of the gas phase reaction of the cyclohexyl radical with dioxygen using a distonic radical ion approach, J. Phys. Chem. A 114 (2010) 1446–1456.

[50] D. G. Harman, S. J. Blanksby, Trapping of a *tert*-adamantyl peroxyl radical in the gas phase, Chem. Commun. 8 (2006) 859–861.

[51] L. Joly, R. Antoine, A. Allouche, P. Dugourd, Formation and spectroscopy of a tryptophan radical containing peptide in the gas phase, J. Am. Chem. Soc. 130 (2008) 13832–13833.

[52] L. Joly, R. Antoine, M. Broyer, J. Lemoine, P. Dugourd, Electron photodetachment from gas phase peptide dianions. relation with optical absorption properties, J. Phys. Chem. A 112 (2008) 898–903.